Analysis of an Induction Heating System by the Finite Element Method Combined with a Boundary Integral Equation

TANROKU MIYOSHI, MEMBER, IEEE, MUNEHIKO SUMIYA, AND HIDEKI OMORI, MEMBER, IEEE

Abstract—**The method, based upon the finite element technique, is presented for the analysis of an induction heating system in unbounded free space. In the induction system, a quasistatic magnetic field problem with cylindrical symmetry is solved. First, a mathematical boundary is defined arbitrarily in free space to contain an induction system inside. An integral relation is derived on the boundary surface using the response function excited by a circular line current. The boundary relation gives a constraint to the finite element analysis in the interior region. In the finite element discretization, first-order elements are used, and constant elements are assumed for the discretization of the boundary equation. To couple the finite element analysis to the boundary integral equation, only the potentials differently approximated on the boundary are matched reasonably. After the accuracy of the method is verified for a single coil, load characteristics of a practical induction heating system are analyzed.**

I. Introduction

IN THE BASIC arrangement of an induction heating system consisting of an exciting coil and a conducting circular plate, the boundaries are not always closed but unbounded in free space. We proposed before the field analysis based upon the finite element method (FEM) to model exterior open regions satisfactorily [1]. The basic technique of the method was to draw a mathematical sphere to enclose an induction heating system. The exterior energy functional was given in a simple form by expanding exterior fields in terms of the solutions of a differential equation governing exterior empty spaces. The interior and exterior potentials were matched at the nodal points on the spherical interface. The magnetic flux leakage from an induction heating system and its reduction by a conducting ring were discussed using the method proposed [2].

In this paper, the alternative method is presented to analyze the unbounded field problem based upon FEM. It would give more freedom in the choice of mathematical boundaries and hence make the interior region to which the FEM is applied smaller. First, an arbitrary mathematical boundary is defined in free space to contain an induction heating system inside. An integral relation is derived on the boundary surface using the response function excited by a circular line current. The boundary relation gives a constraint to the FEM analysis in the interior region. The method similar to this approach was presented first by McDonald and Wexler in [3], [4] and modified in [5] for the two-dimensional electromagnetic field problems, although a different way of boundary constraint was formulated to cope with the singularities of Green's functions. The general principle to combine the finite element and the boundary integral formulation has been developed by Salon *et al.* in [6]–[8]. Our paper is an application of the general principle to a problem of practical importance.

In the analysis of the induction system, the axisymmetric problem of quasistatic magnetic fields is solved. For the discretization of the boundary integral equation, constant elements [9] are used in this paper, where both the potential and the flow on the boundary are assumed to be constant over each section between the nodal points. On the other hand, in the FEM discretization, first-order elements are used. Since the approximate functions of potentials are different in two discretizations, the matching process of potentials is necessary to combine two solutions. The flow is guaranteed to be continuous across each section in the above approximation because first-order FEM elements give constant flows on the boundary.

After the accuracy of the method described above is verified for a single coil, load characteristics of a practical induction heating system are analyzed.

II. Analysis

The basic system of an induction heating to be analyzed in this paper is illustrated in Fig. 1. In the system, alternating magnetic fields produced by an exciting coil induce eddy currents in a conducting circular plate above the coil. Eddy currents flow in circular paths and give rise to a heating effect in the plate.

To analyze the system in free space, we first draw a mathematical boundary S to enclose the system as shown in dashed lines in Fig. 1. Because of the cylindrical symmetry of the structure, the surface of a cylinder is taken as the boundary. The FEM is applied only inside the cylinder.

Manuscript received May 4, 1986; revised September 8, 1986.

T. Miyoshi and M. Sumiya are with the Department of Electronic Engineering, Kobe University, Rokko, Nada, Kobe 657, Japan.

H. Omori is with the Engineering Development Center, Home Appliance Sector, Matsushita Electric Industrial Company, Hinode, Toyonaka, Osaka 561, Japan.

IEEE Log Number 8612900.

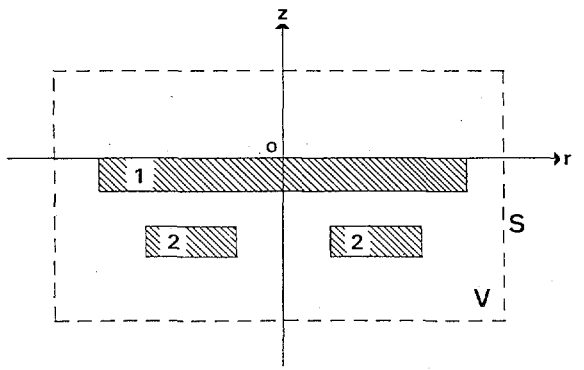

Fig. 1. Basic arrangement of induction heating system and mathematical boundary. "1" is the ferromagnetic circular plate, and "2" is the exciting coil.

A. Formulation of FEM

In the above system only the angular components of the current density and the magnetic vector potential are considered and denoted by J and A, respectively. They are all assumed to have the conventional exp ($j\omega t$) harmonic time dependence. For the axisymmetric problem of quasi-static magnetic fields, the following form of equation holds in cylindrical coordinate system (r, θ, z):

$$\nabla^2 A - \frac{A}{r^2} = -\mu J, \qquad \nabla^2 = \frac{\partial^2}{\partial r^2} + \frac{1}{r}\frac{\partial}{\partial r} + \frac{\partial^2}{\partial z^2} \tag{1}$$

where μ denotes the permeability of the conducting plate. J is given by $-j\omega\sigma A$ in the plate with the conductivity σ and by zero in empty spaces. For simplicity the normal derivatives of A on the boundary are represented from now on as

$$\frac{\partial A}{\partial n} = q. \tag{2}$$

Then the energy functional I, which is the variational representation of (1), is given by

$$I = \int_V \frac{1}{\mu}\left\{ |\nabla A|^2 + \frac{|A|^2}{r^2} \right\} dV - \int_V (JA^* + J^*A)\, dV - \frac{1}{\mu_0}\int_S \{A^* q^{(F)} + A q^{(F)*}\}\, dS \tag{3}$$

where the asterisk means a complex conjugate and

$$\nabla = \frac{\partial}{\partial r} i_r + \frac{\partial}{\partial z} i_z.$$

$q^{(F)}$ will be shown to satisfy the integral relation between q and A on the boundary in the next section.

For the discretization of the functional I, the interior region is subdivided into axisymmetric triangular elements. Let A_i be the nodal potential of the ith vertex and ξ_i the first order approximate function in the kth element, then an approximate solution in this element is constructed by the equation

$$A = \sum_{i=1}^{3} \xi_i A_i \tag{4}$$

where by definition ξ_i takes on the values of one only at node i and zero at other nodes. The functional I_k for the kth element is approximated by using (4) as

$$I_k = \sum_{i=1}^{3}\sum_{j=1}^{3} A_i A_j^* S_{ij} - \sum_{i=1}^{3} (A_i^* T_i + A_i T_i^*) - \sum_{i=1}^{3} \{A_i^* D_{ik} q_k^{(F)} + A_i D_{ik} q_k^{(F)*}\} \tag{5}$$

where

$$S_{ij} = 2\pi \int \frac{r}{\mu} \nabla\xi_i \cdot \nabla\xi_j\, dr\, dz + 2\pi \cdot \int \frac{1}{\mu r} \xi_i \xi_j\, dr\, dz + 2\pi \int j\omega\sigma r \xi_i \xi_j\, dr\, dz \tag{6}$$

$$T_i = 2\pi \int Jr\xi_i\, dr\, dz \tag{7}$$

$$D_{ik} = \frac{2\pi}{\mu_0} \int r\xi_i\, ds_k. \tag{8}$$

Here T_i take values only for the elements inside the coil. D_{ik} is not zero only for the nodal points on the boundary. Further, it should be noted that both the vector potentials and their normal derivatives on the central axis always vanish due to the cylindrical symmetry of the structure. The total functional I is approximated by the sum of I_k in (5) for every element. The stationary points of I can be selected by evaluating the equations $\partial I / \partial A_i^*$ for every nodal point. This immediately gives the following matrix equation:

$$\begin{bmatrix} [S_{II}] & [S_{IC}] \\ [S_{CI}] & [S_{CC}] \end{bmatrix} \begin{bmatrix} \{A\}_I^{(F)} \\ \{A\}_C^{(F)} \end{bmatrix} = \begin{bmatrix} \{T\} \\ [D]\{q\}_C^{(F)} \end{bmatrix} \tag{9}$$

where the nodal vector potentials are divided into two parts and written as $\{A\}_I^{(F)}$ and $\{A\}_C^{(F)}$. $\{A\}_I^{(F)}$ denotes the vector for the nodes inside the region, and $\{A\}_C^{(F)}$ denotes the vector for the nodes on the boundary.

B. Boundary Integral Equation

The vector potential in free space satisfies the following equation as explained in (1)

$$\nabla^2 A - \frac{A}{r^2} = 0. \tag{10}$$

We now introduce the response function G satisfying

$$\nabla^2 G - \frac{G}{r^2} = -\delta(r - r_0, z - z_0). \tag{11}$$

The free space response function that is the vector potential at (r, z) excited by a circular line current at (r_0, z_0) is known as [10]

$$G(r, r_0/z, z_0) = \frac{1}{\pi k}\sqrt{\frac{r_0}{r}}\left\{\left(1 - \frac{k^2}{2}\right) K(k) - E(k)\right\} \tag{12}$$

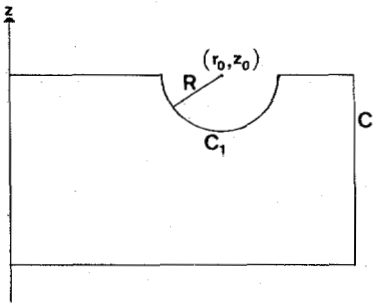

Fig. 2. Path of integration around a singular point on the boundary.

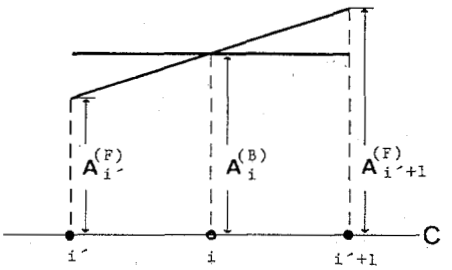

Fig. 3. Approximate functions of vector potentials on the boundary. ● denotes the nodal point used in the FEM, and ○ is the sampling point used in the boundary integral equation.

where $K(k)$ and $E(k)$ denote the complete elliptic integrals of the first and second kinds, respectively, and k is given by

$$k^2 = 4rr_0/[(r + r_0)^2 + (z - z_0)^2]. \quad (13)$$

Multiplying (10) by G, (11) by A, subtracting the resulting equations, and integrating over the exterior region, we obtain

$$\int_S \left(G\frac{\partial A}{\partial n} - A\frac{\partial G}{\partial n} \right) dS = 2\pi r_0 A(r_0, z_0) \quad (14)$$

where Green's theorem is applied. Further, considering that A and G are constant in the angular direction, (14) is rewritten as

$$\int_C \left(G\frac{\partial A}{\partial n} - A\frac{\partial G}{\partial n} \right) r\, ds = r_0 A(r_0, z_0) \quad (15)$$

for any point (r_0, z_0) in the exterior region on the r-z plane.

When we apply (15) to the point (r_0, z_0) just on the boundary, a little algebra is required because of the singularity of the response function. A minute semicircle C_1 with radius R is now described having the center at (r_0, z_0) as shown in Fig. 2. On the semicircle, because $k \fallingdotseq 1$ from (13), using the approximations of $K(k) \fallingdotseq \ln(8r_0/R)$ and $E(k) \fallingdotseq 1$, the response function and its normal derivative are approximated by

$$G = \frac{1}{\pi}\left(\frac{1}{2} \ln \frac{8r_0}{R} - 1 \right), \qquad \frac{\partial G}{\partial n} = \frac{\partial G}{\partial R} = -\frac{1}{2\pi R}. \quad (16)$$

Then, the integration along C_1 in (15) are obtained as follows:

$$\int_{C_1} A\frac{\partial G}{\partial n} r\, ds = -\frac{1}{2} r_0 A(r_0, z_0) \quad (17)$$

$$\int_{C_1} G\frac{\partial A}{\partial n} r\, ds = \frac{\partial A}{\partial n} r_0 R\left(\frac{1}{2} \ln \frac{8r_0}{R} - 1 \right). \quad (18)$$

Next, when R tends to zero, the right side of (18) vanishes and hence (15) results in the following integral equation in terms of A and $\partial A/\partial n$:

$$\int_C \left(G\frac{\partial A}{\partial n} - A\frac{\partial G}{\partial n} \right) r\, ds = \frac{1}{2} r_0 A(r_0, z_0). \quad (19)$$

For the discretization of (19), we divide the boundary into sections by the nodal points used in the FEM and set sampling points defined at the center of each section. When we assume that A and $\partial A/\partial n$ are uniform across each section, the above integral equation results in a matrix equation:

$$[F]\{q\}^{(B)}_C - [H]\{A\}^{(B)}_C = \{0\}. \quad (20)$$

The elements of the matrices $[F]$ and $[H]$ are given by

$$F_{ij} = \begin{cases} \displaystyle\int_{C_j} Gr\, ds = G_{ij} r_j w_j, & i \neq j \\ \displaystyle\frac{w_i r_i}{2\pi}\left(\ln \frac{16 r_i}{w_i} - 1 \right), & i = j \end{cases} \quad (21)$$

$$H_{ij} = \begin{cases} \displaystyle\int_{C_j} \frac{\partial G}{\partial n} r\, ds = \left(\frac{\partial G}{\partial n} \right)_{ij} r_j w_j, & i \neq j \\ \displaystyle\frac{1}{2} r_i, & i = j \end{cases} \quad (22)$$

where r_i denotes the r coordinate of the ith sampling point and w_i is the length of the ith section. G_{ij} and $(\partial G/\partial n)_{ij}$ in (21) and (22), respectively, are formulated easily by using (12) because $\partial G/\partial n$ takes the values computed from $\partial G/\partial r$ and $\partial G/\partial z$, which correspond to the position of the observing point on the boundary.

C. Coupling of the FEM to the Boundary Integral Equation

In Sections II-A and II-B, the different approximate functions of vector potentials are used in the discretizations. In the FEM discretization, first-order elements are used and constant elements are assumed for the discretization of the boundary integral equation. On the other hand, the normal derivatives across each section on the boundary are guaranteed to be continuous in the discretizations because first-order FEM elements give constant flows on the boundary:

$$\{q\}^{(F)}_C = -\{q\}^{(B)}_C. \quad (23)$$

Consequently, to couple the FEM analysis to the boundary integral equation, only the vector potentials differently approximated on the boundary should be matched reasonably. It is easy to understand from Fig. 3 that the

following relation must apply to make the average potential over each section equal. Thus

$$A_i^{(B)} = \tfrac{1}{2}\left\{A_{i'}^{(F)} + A_{i'+1}^{(F)}\right\} \tag{24}$$

where the superscripts (F) and (B) correspond to the FEM analysis and the boundary integral equation, respectively. In a matrix form, the relations are written as

$$\{A\}_C^{(B)} = [C]\{A\}_C^{(F)} \tag{25}$$

where $[C]$ is constructed only by the components of zero or one half. Coupling the three matrix equations (9), (20), and (25), we can finally obtain

$$\begin{bmatrix} [S_{II}] & [S_{IC}] \\ [S_{CI}] & [S_{CC}] + [D][F]^{-1}[H][C] \end{bmatrix} \times \begin{bmatrix} \{A\}_I^{(F)} \\ \{A\}_C^{(F)} \end{bmatrix} = \begin{bmatrix} \{T\} \\ \{0\} \end{bmatrix}. \tag{26}$$

The equation indicates that the vector potentials in the interior region are determined only if the excited currents of the coil are given.

III. Numerical Results

A. Single Coil with Square Cross Section

As an example of the method described, the magnetostatic fields due to a single coil with square cross section shown in Fig. 4 are computed first to check the computation accuracy. The current distributions are assumed to be uniform throughout the cross section. A total of 240 of axisymmetric triangular elements are used to divide the interior region, and 32 nodes are set on the boundary. The computed nodal vector potentials along the mathematical boundary are shown in Fig. 5 and compared with the analytic solutions that are determined by the integration of (12) over the cross section of the coil. Discrepancies are observed around the boundary near the coil, but the computational error is within about 3.6 percent.

Inductance L of the coil will give another measure of the computational accuracy for this problem. L is known to be computed from the magnetic energy functional (3) if it is multiplied by $2/(\text{total current})^2$. However, since it is the variational representation of inductance, this method should not be applicable to check the accuracy of the computed potentials. Therefore, inductance is computed here from the input voltage when the total exciting current is taken to have unity value:

$$L = \frac{1}{S}\int_{\text{coil}} 2\pi r A(r, z)\, dr\, dz. \tag{27}$$

The computed inductance is found to be 0.185 μH while the exact inductance determined by the analytic solutions is given as 0.189 μH.

B. Induction Heating System

Before analyzing the practical induction heating system, a simple induction heating model shown in Fig. 6 is tested first. In the induction heating system, since fields are expected to be concentrated strongly around the surface of the ferromagnetic conducting plate due to skin effect, axisymmetric triangular elements with height about a half of skin depth are arranged along the inside surface of the conductor. In calculation, 708 elements are used in

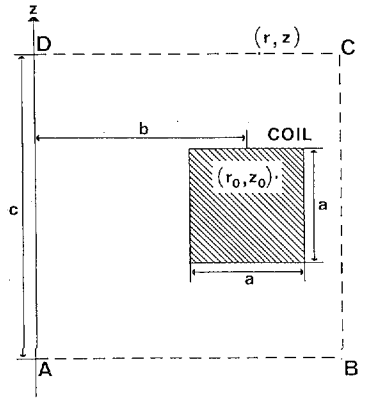

Fig. 4. Single coil with square cross section. a = 2 cm, b = 7 cm, and c = 10 cm.

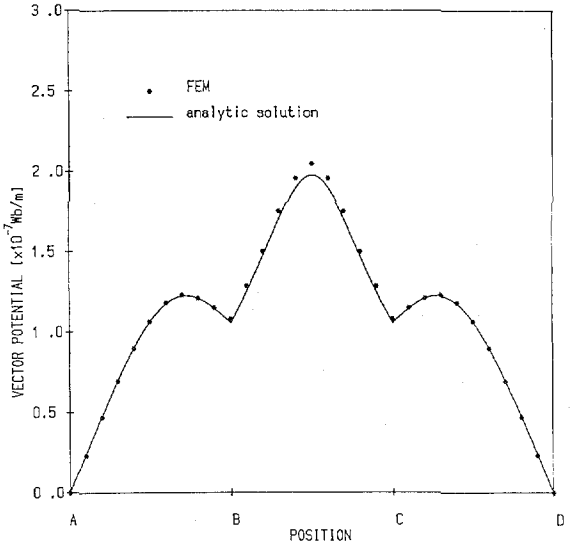

Fig. 5. Computed nodal vector potentials along the mathematical boundary compared with the analytic solutions, A, B, C, and D on the abscissa indicate the positions on the boundary shown in Fig. 4.

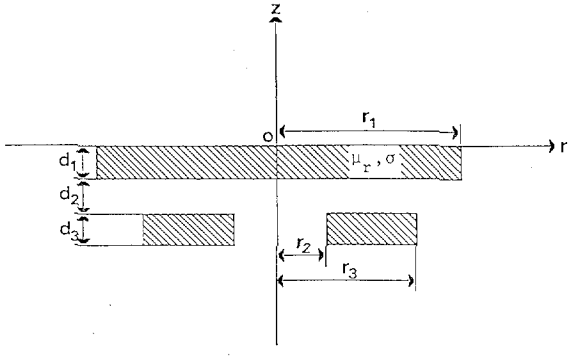

Fig. 6. Simple induction heating model. r_1 = 16 cm, r_2 = 2 cm, r_3 = 11 cm, d_1 = 2 mm, d_2 = 8 mm, d_3 = 5 mm, $\sigma = 3.61 \times 10^6$ S/m.

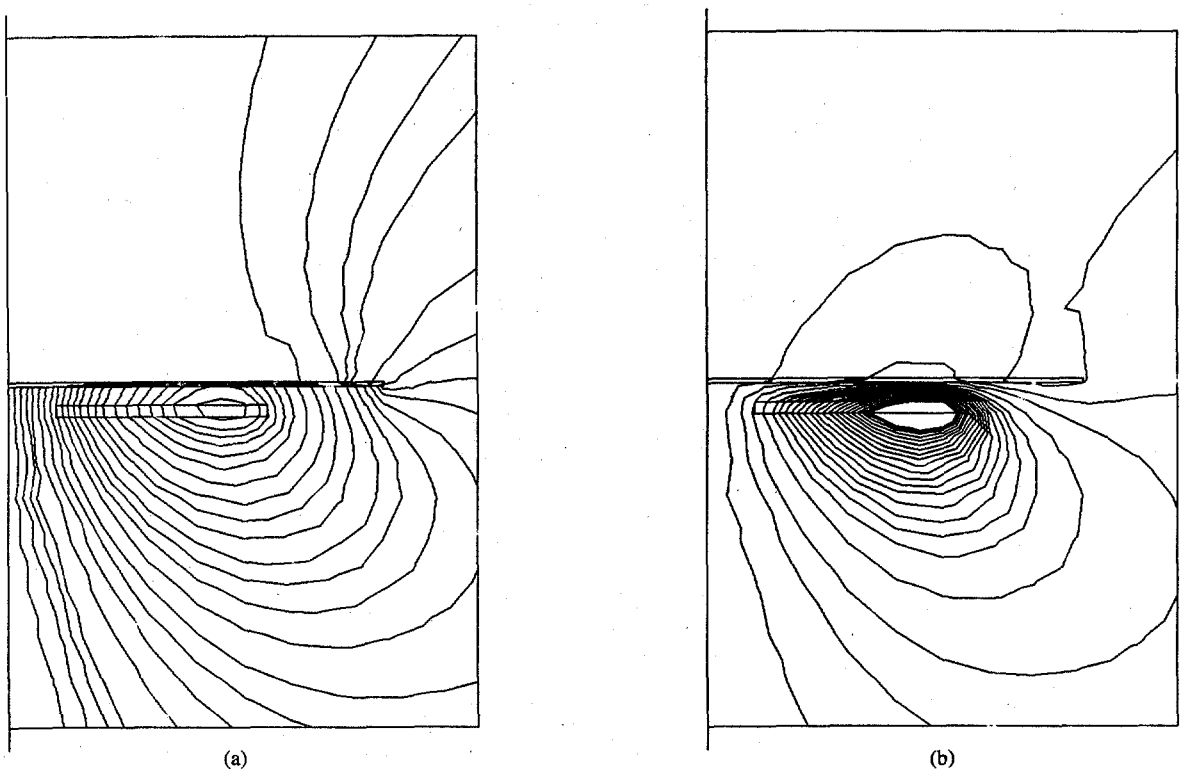

Fig. 7. Computed magnetic field-distributions at 20 kHz. (a) Ferromagnetic conducting plate with $\mu_r = 1270$. (b) Normal conductor with $\mu_r = 1$.

the interior region and 37 nodes are set on the boundary. The computed magnetic field distributions are illustrated in Fig. 7(a) and (b) for ferromagnetic and normal conducting plates, respectively. They show the distributions at the operating frequency of 20 kHz. In Fig. 7(a) for ferromagnetic plate with relative permeability $\mu_r = 1270$, the magnetic fields are found to be concentrated to the bottom of the plate with the skin depth of 0.05 mm. On the contrary, for the normal conducting plate with $\mu_r = 1$, due to the relatively thick skin depth of 1.9 mm, a large amount of currents induced inside the plate push out the magnetic flux from the plate, cancelling the originally excited magnetic fields. Further, there is more leakage of magnetic flux over the top of the plate because of the weaker shielding effect of the normal conductor.

Next, the practical induction heating system with more complicated cross section shown in Fig. 8 is analyzed. A ferrite disk placed under the coil is practically used for shielding strong magnetic fields produced by the exciting coil. In the analysis, two mathematical boundaries are defined in the induction system. One contains the exciting coil and the ferrite disk, and the other contains only the vessel. When the separation between the two regions is varied to analyze the load characteristics of the exciting coil as a function of distance between the vessel and the exciting coil, the numerical method mentioned before is applied without any change of the finite elements in the interior regions. In calculation, 790 elements are used in the interior region and 220 nodes are set on the boundary.

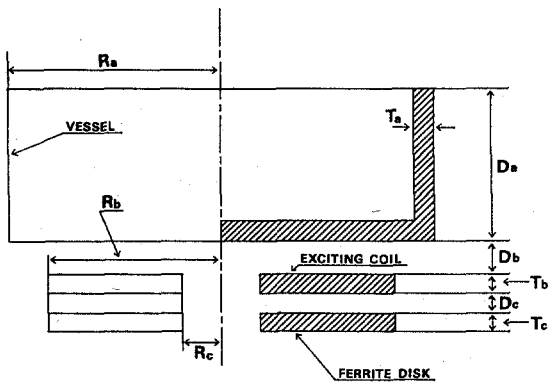

Fig. 8. Practical induction heating system. $R_a = 98$ mm, $R_b = 90$ mm, $R_c = 25$ mm, $T_a = 1.2$ mm, $T_b = 3$ mm, $T_c = 5$ mm, $D_a = 79$ mm, $D_b = 10$ mm, $D_c = 2.5$ mm. Vessel: $\mu = 6.28 \times 10^{-4}$ H/m, $\sigma = 1.02 \times 10^7$ S/m. Ferrite: $\mu = 1.69 \times 10^{-3}$ H/m, $\sigma = 0$. Coil: 22 turns.

In order to determine the input impedance Z of the exciting coil, the input voltage is calculated from the following equation when the input current is taken to have unity value:

$$Z = \frac{j\omega N}{S} \int_{\text{coil}} 2\pi r A(r, z)\, dr\, dz \tag{28}$$

where N is the number of turns of the exciting coil and S denotes the total cross section of the coil. If the input impedance is represented simply as $Z = R + j\omega L$, the variation of R and L as a function of the distance D_b between the vessel and the exciting coil are computed as

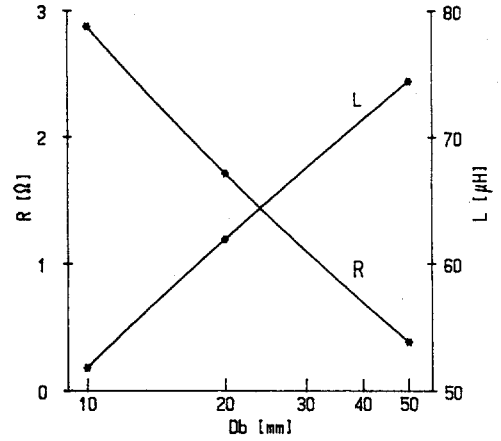

Fig. 9. Input impedance of the exciting coil as a function of distance D_b between the vessel and the exciting coil $Z = R + j\omega L$.

shown in Fig. 9 at 25 kHz. R is found to decrease with distance because the induced current decreases with distance, which makes the power dissipation in the vessel smaller. On the other hand, L increases with distance. This is due to the fact that the original magnetic fields excited by the coil are cancelled less by the smaller induced current in the vessel as the separation increases. In the limit of infinity of the separation, L approaches to 74.4 μH, which is the inductance of the exciting coil without any load in free space.

A real equivalent circuit describing the induction heating would be more complicated than that discussed here. A mutual coupling circuit model may be a candidate for a one-port equivalent circuit to represent the load characteristics of the exciting coil. We will study this model further in order to design the inverter circuits that drive the induction heating system.

IV. Conclusion

The FEM combined with the boundary integral equation has been discussed to solve the magnetoquasistatic unbounded problems with cylindrical symmetry. The approach described here is superior to the method proposed before in the sense that the mathematical boundary can be defined arbitrarily. The method has been applied well to obtain load characteristics of a practical induction heating system. The load characteristics of an exciting coil may be important in the design of the inverter circuits that drive the induction heating system.

References

[1] T. Miyoshi and G. Maeda, "Finite element analysis of leakage magnetic flux from an induction heating system," *IEEE Trans. Magn.*, vol. MAG-18, pp. 917-920, May 1982.

[2] T. Miyoshi, H. Omori, and G. Maeda, "Reduction of magnetic flux leakage from an induction heating range," *IEEE Trans. Ind. Appl.*, vol. IA-19, pp. 491-497, July 1983.

[3] B. H. McDonald and A. Wexler, "Finite-element solution of unbounded field problems," *IEEE Trans. Microwave Theory Tech.*, vol. MTT-20, 12, pp. 841-847, Dec. 1972.

[4] M. V. Chari and P. P. Silvester, *Finite Elements in Electrical and Magnetic Field Problems*. New York: John Wiley, chap. 9, 1980.

[5] S. Washisu, I. Fukai, and M. Suzuki, "Extension of finite-element method to unbounded field problems," *Electron. Lett.*, vol. 15, 24, pp. 772-774, Nov. 1979.

[6] S. J. Salon and J. M. Schneider, "A hybrid finite element-boundary integral formulation of Poisson's equation," *IEEE Trans. Magn.*, vol. MAG-17, pp. 2574-2576, Nov. 1981.

[7] S. J. Salon and J. M. Schneider, "A hybrid finite element-boundary integral formulation of the eddy current problem," *IEEE Trans. Magn.*, vol. MAG-18, pp. 461-466, Mar. 1982.

[8] S. J. Salon and J. P. Peng, "A hybrid finite element-boundary element formulation of Poisson's equation for axisymmetric vector potential problems," *J. Appl. Phys.*, vol. 53, pp. 8420-8422, Nov. 1982.

[9] T. Okoshi and T. Miyoshi, "The planar circuit—an approach to microwave integrated circuitry," *IEEE Trans. Microwave Theory Tech.*, vol. MTT-20, pp. 245-252, Apr. 1972.

[10] J. A. Stratton, *Electromagnetic Theory*. New York: McGraw-Hill, p. 262, 1941.

Tanroku Miyoshi (S'67-M'72) was born in Osaka, Japan, on January 6, 1944. He received the B.S., M.S., and Ph.D. degrees in electronic engineering from the University of Tokyo, Japan, in 1967, 1969, and 1972, respectively.

In 1972 he was appointed Lecturer, and since 1974 he has been an Associate Professor in the Department of Electronic Engineering, Kobe University, Kobe, Japan. He has been engaged in research of electomagnetic theory and microwave and optical devices. In 1976 he was a Visiting Scholar at McGill University, Montreal, PQ, Canada. From 1982 to 1984, he was a Visiting Consultant at Bell Laboratories, Holmdel, NJ.

Dr. Miyoshi is a member of the Institute of Electrical and Electronics Engineers, the Institute of Electronics and Communication Engineers of Japan, and the Institute of Electrical Engineers of Japan. He received a Yonezawa Award in 1974 and Outstanding Book Award in 1977 both from the Institute of Electronics and Communication Engineers of Japan.

Munehiko Sumiya was born in Wakayama, Japan, on November 23, 1963. He received the B.S. degree in electrical engineering from Kobe University, Kobe, Japan, in 1986.

He is presently completing the requirements for the M.S. degree in electronic engineering at Kobe University.

Mr. Sumiya is an associate member of the Institute of Electrical Engineers of Japan.

Hideki Omori (M'85) was born in Hyogo, Japan, on May 2, 1954. He received the B.S. and M.S. degrees in electronic engineering from Kobe University, Kobe, Japan, in 1975 and 1977, respectively.

Since joining the Home Appliance Research Laboratory, Matsushita Electric Industrial Company in 1977, he has been engaged in developmental research on induction heating ranges.

Mr. Omori is a member of the Institute of Electrical Engineers of Japan and the Institute of Electronics and Communication Engineers of Japan.